Applied Acoustics 116 (2017) 43–49

Contents lists available at ScienceDirect

Applied Acoustics

journal homepage: www.elsevier.com/locate/apacoust

Technical note

Axisymmetric fluid-dominated wave in fluid-filled plastic pipes: Loading effects of surrounding elastic medium

Yan Gao [a,*], Yuyou Liu [b,c], Jennifer M. Muggleton [d]

[a] Key Laboratory of Noise and Vibration Research, Institute of Acoustics, Chinese Academy of Sciences, Beijing 100190, China
[b] Beijing Municipal Institute of Labour Protection, Beijing 100054, China
[c] Environment & Ground Engineering, UK & Ireland, AECOM, London SW19 4DR, UK
[d] Institute of Sound and Vibration Research, University of Southampton, Southampton SO17 1BJ, UK

ARTICLE INFO

Article history:
Received 27 June 2016
Received in revised form 8 September 2016
Accepted 12 September 2016

Keywords:
Fluid-filled pipe
Acoustics
Wavenumber
Elastic medium

ABSTRACT

Axisymmetric ($n = 0$) waves that propagate at low frequencies are of practical interest in the application of acoustic techniques for the detection of leaks in fluid-filled pipelines. A general expression for the fluid-dominated ($s = 1$) wavenumber is presented in a thin-walled fluid-filled pipe surrounded by an elastic medium. In this paper the analysis is extended to investigate the loading effects of surrounding medium on the low-frequency propagation characteristics of the $s = 1$ wave. The analytical model is subsequently applied to MDPE water pipes surrounding by three media, namely an air, water and soil. It is used to demonstrate explicitly the loading effects of surrounding medium, acting as a combination of mass, stiffness and radiation damping on the $s = 1$ wavenumber. Good agreement is achieved between the measurements and predictions. The theory with experimental validations provides the basis for improving acoustic leak detection methods in fluid-filled pipe systems.

1. Introduction

Cylindrical pipes are the practical elements for transporting fluids and gases in the petrochemical, water and energy industries. Leakage from pipes has been a major issue for some time due to the social, environmental and economic consequences. Acoustic techniques have been shown to be effective for the detection of leaks in fluid-filled pipes [1–6]. In particular, methods based on cross-correlation provide a powerful solution for locating water leaks, and are now in common use in many countries. For these methods to be effective, the propagation characteristics of the dominant waves need to be know *a priori*. Plastic pipes are now being increasingly used in many water distribution systems in China and around the world. Although cross-correlation methods have been used successfully to identify the location of water leaks in metal pipes, they are less effective in plastic pipes. In practical leak detection surveys, water leaks can be detected in metal pipes at large ranges (upwards of 1 km). This may be reduced by a factor of 10 or more for plastic pipes. The dominant wave types that propagate in fluid-filled pipes must be better understood in order to meet the challenge of significantly improving water leakage detection ranges, in particular for plastic pipes.

Much research has been devoted to studying the wave propagation and energy distribution within elastic fluid-filled pipes *in vacuo* by solving wave equations under the boundary conditions for thin-walled shells. In earlier research, Lin and Morgan [7] studied the axisymmetric ($n = 0$) waves through fluid contained in an elastic thin cylindrical shell. Fuller and Fahy [8] derived the $n = 0$ wavenumbers for fluid-filled pipes defined as "hard" and "soft" shells, and Xu and Zhang [9] investigated the forced vibration. Fuller [10] studies theoretically the energy distribution among various wave types for a radial wall input force and for internal pressure pulsations. Pinnington and Briscoe [11] introduced an external circumferential piezoelectric transducer to detect the radial wall motion of a fluid-filled pipe. Pinnington [12,13] further investigated the $n = 0$ wave transmission properties and transfer functions for pressurized flexible tubes.

Recent research has shown that at low frequencies, one particular $n = 0$ wave, namely, the fluid-dominated ($s = 1$) wave is often the main carrier of the vibrational energy in buried fluid-filled plastic pipes [14–16]. In this special case where $n = 0$, $s = 1$ corresponds to a breathing mode (or no motion at all) of the pipe shell in the circumferential direction. The cited work suggests that relatively predictable for metal pipes, the acoustic characteristics of

* Corresponding author.
E-mail address: gaoyan@mail.ioa.ac.cn (Y. Gao).

http://dx.doi.org/10.1016/j.apacoust.2016.09.016
0003-682X/

wave propagation are largely unknown for plastic pipes, due to the uncertainties in the propagation wavespeed and the radiation damping effect on the attenuation. Additionally, strong coupling between the pipe wall, the contained fluid and the surrounding soil occurs in buried fluid-filled plastic pipes. Muggleton et al. [14–16] developed theoretical models and conducted some experiments to validate the predictions for the $s = 1$ wave. However, the soil medium was not appropriately modelled: it was treated as a fluid effectively supporting the elastic waves in the soil [14]; the effects of soil were taken into account under a lubricated contact condition [16]. However in reality some shear stress will always be present at the interface. In particular, neglecting the frictional stress is questionable for the purpose of attenuation predictions.

The present authors [17] have recently developed an analytical method for investigating the dispersion characteristics of the $s = 1$ wave motion in buried fluid-filled pipes. In this paper, the analysis is extended to study the loading effects of surrounding elastic medium, acting as a combination of mass, stiffness and radiation damping, on the propagation characteristics of the $s = 1$ wave. Theoretical predictions of the $s = 1$ wavenumber are compared with wavenumber measurements made on actual medium density polyethylene (MDPE) water pipes in-air, in-water and buried in sandy soil.

2. Theory

2.1. The s = 1 wavenumber

This section derives a general expression for the $n = 0$, $s = 1$ wavenumber in a fluid-filled pipe surrounded by an elastic medium. In the analysis, the fluid-filled pipe system is modelled as a cylindrical tri-layer system with the cross-section as shown in Fig. 1. The inner layer of fluid cannot support shear, and the pipe wall is modelled based on the thin shell theory while the outer layer of an elastic medium may support both compressional and shear motions without loss of generality. The problems we shall consider concern the propagation of elastic disturbances in layered media, each layer satisfying the continuity conditions at the interfaces.

We begin with a brief outline of the coupled axial and radial motion of the fluid-filled pipe with a mean radius a and wall thickness h such that $h/a \ll 1$. Referring to Fig. 2, u and w denote the displacements of the shell element in the x and r directions, respectively. The internal fluid is assumed to be inviscid and the surrounding elastic medium is homogenous and isotropic. Losses within the fluid and surrounding media are both neglected. Coupled equations of motion for the $n = 0$ waves that propagate in a buried fluid-filled pipe have been derived with a more detailed treatment may be found in [17]. For each s wave, the travelling wave solutions of the form $u = U_s e^{i(\omega t - k_s x)}$ and $w = W_s e^{i(\omega t - k_s x)}$ and $p_f = P_{fs} J_0\left(k_{fs}^r r\right) e^{i(\omega t - k_s x)}$ are used to describe the pipe wall displacements and internal pressure, where k_s is the axial wavenumber; U_s and W_s are the amplitudes of shell displacements in the axial and radial directions respectively; P_{fs} is the amplitude of the internal pressure; the internal fluid radial wavenumber, k_{fs}^r, is related to the free-field fluid wavenumber, k_f, by $\left(k_{fs}^r\right)^2 = k_f^2 - k_s^2$ and $k_f^2 = \omega^2 \rho_f / B_f$; B_f and ρ_f are the bulk modulus and density of the contained fluid; ω is the angular frequency; and $J_0()$ represents a Bessel function of order zero.

Consider the equations governing the coupled axial and radial motion for the axisymmetric s waves in a fluid-filled pipe surrounded by an elastic medium [17]

$$\begin{bmatrix} \Omega^2 - (k_s a)^2 - SL_{11} & -i\nu_p (k_s a) - SL_{12} \\ -i\nu_p (k_s a) - SL_{21} & 1 - \Omega^2 - FL - SL_{22} \end{bmatrix} \begin{bmatrix} U_s \\ W_s \end{bmatrix} = \mathbf{0} \tag{1}$$

where Ω is the nondimensional frequency, $\Omega = k_L a$; k_L is the shell compressional wavenumber, $k_L^2 = \omega^2 \rho_p \left(1 - \nu_p^2\right)/E_p$; ρ_p, E_p and ν_p are the density, Young's modulus and Poisson's ratio of the shell; FL and **SL** are the fluid loading term and the loading matrix of surrounding medium representing the coupling effects of the contained fluid and surrounding medium on the pipe wall respectively. Referring to Fig. 1, the contained fluid applies the pressure at the pipe-fluid interface and the surrounding medium applies the stresses in the axial and radial directions at the pipe-medium interface. Applying the momentum equation and the displacement

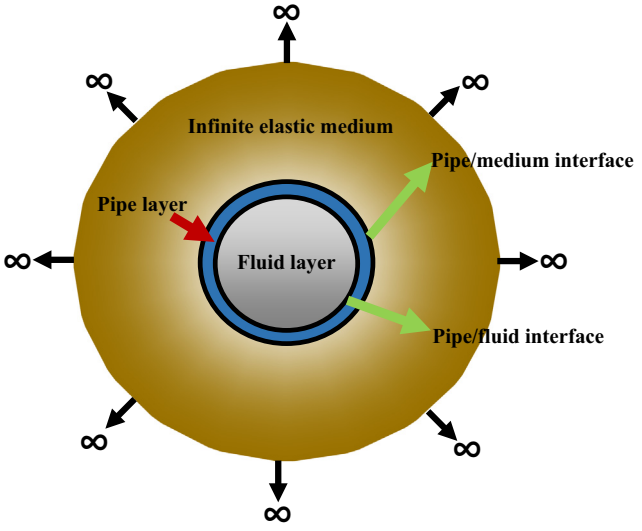

Fig. 1. Schematic of the cross-section of a fluid-filled pipe surrounded by an infinite elastic medium.

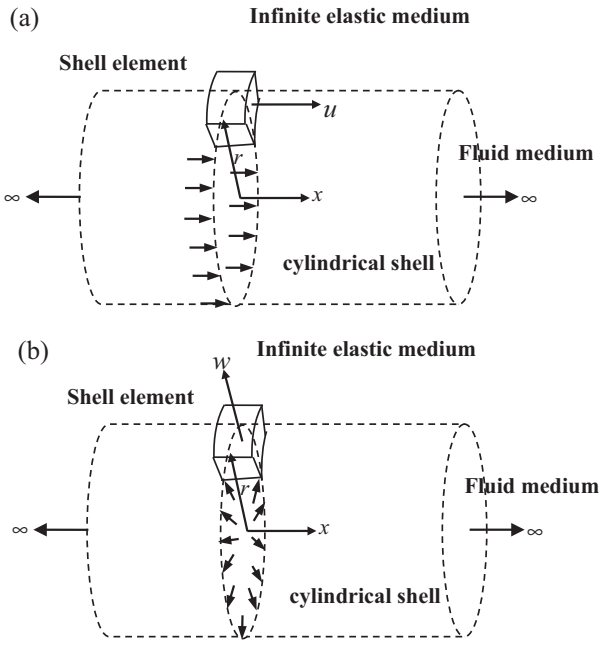

Fig. 2. Schematic of the coupled axial and radial motion of the shell element of radius a and thickness h in cylindrical coordinates: (a) in the axial direction; (b) in the radial direction.

continuity in the radial direction at the pipe-fluid interface, the fluid loading term *FL* was first introduced by Fuller and Fahy, which is given by [8]

$$FL = \frac{\rho_f}{\rho_p}\frac{a}{h}\frac{\Omega^2}{k_{fs}^r a}\frac{\mathrm{J}_0\left(k_{fs}^r a\right)}{\mathrm{J}_0'\left(k_{fs}^r a\right)} \tag{2}$$

where $\mathrm{J}_0' = (\partial/\partial r)\mathrm{J}_0()$. At low frequencies, the approximation for the Bessel function ratio may be adopted, i.e., $\mathrm{J}_0(x)/\mathrm{J}_0'(x) \approx -2/x$ when $x \to 0$. Thus Eq. (2) is approximated by

$$FL = -2\frac{\rho_f}{\rho_p}\frac{a}{h}\frac{\Omega^2}{k_f^2 a^2 - k_s^2 a^2} \tag{3}$$

Applying the displacement continuity in the axial and radial directions at the pipe-medium interface, the loading matrix, **SL**, is found to be obtained by [17]

$$\left.\begin{aligned} SL_{11} &= -\mu_m \frac{(1-\nu_p^2)}{E_p}\frac{a}{h}\frac{k_{ds}^r a k_{rs}^2 a^2}{k_{rs}^r a k_{ds}^r a\left[\mathrm{H}_0\left(k_{rs}^r a\right)/\mathrm{H}_0'\left(k_{rs}^r a\right)\right] + k_s^2 a^2\left[\mathrm{H}_0\left(k_{ds}^r a\right)/\mathrm{H}_0'\left(k_{ds}^r a\right)\right]} \\ SL_{12} &= \mathrm{i}\mu_m \frac{(1-\nu_p^2)}{E_p}\frac{a}{h}k_s a\left\{2 - \frac{k_r^2 a^2 \mathrm{H}_0\left(k_{ds}^r a\right)/\mathrm{H}_0'\left(k_{ds}^r a\right)}{k_{rs}^r a k_{ds}^r a\left[\mathrm{H}_0\left(k_{rs}^r a\right)/\mathrm{H}_0'\left(k_{rs}^r a\right)\right] + k_s^2 a^2\left[\mathrm{H}_0\left(k_{ds}^r a\right)/\mathrm{H}_0'\left(k_{ds}^r a\right)\right]}\right\} \\ SL_{21} &= SL_{12} \\ SL_{22} &= -\mu_m \frac{(1-\nu_p^2)}{E_p}\frac{a}{h}\left\{2 + \frac{k_{rs}^r a k_{rs}^2 a^2\left[\mathrm{H}_0\left(k_{rs}^r a\right)/\mathrm{H}_0'\left(k_{rs}^r a\right)\right]\left[\mathrm{H}_0\left(k_{ds}^r a\right)/\mathrm{H}_0'\left(k_{ds}^r a\right)\right]}{k_{rs}^r a k_{ds}^r a\left[\mathrm{H}_0\left(k_{rs}^r a\right)/\mathrm{H}_0'\left(k_{rs}^r a\right)\right] + k_s^2 a^2\left[\mathrm{H}_0\left(k_{ds}^r a\right)/\mathrm{H}_0'\left(k_{ds}^r a\right)\right]}\right\} \end{aligned}\right\} \tag{4a-d}$$

where the surrounding medium radial wavenumbers, k_{ds}^r and k_{rs}^r, are given by $\left(k_{ds}^r\right)^2 = k_d^2 - k_s^2$, $\left(k_{rs}^r\right)^2 = k_r^2 - k_s^2$ respectively; k_d and k_r are the compressional and shear wavenumbers in the surrounding medium, which are given by $k_d^2 = \omega^2\rho_m/(\lambda_m + 2\mu_m)$ and $k_r^2 = \omega^2\rho_m/\mu_m$ respectively; ρ_m is the density of the surrounding medium, and λ_m and μ_m are the Lamé coefficients; the Hankel functions of the second kind and zero order, $\mathrm{H}_0()$, describe outgoing waves in the surrounding soil; and $\mathrm{H}_0' = (\partial/\partial r)\mathrm{H}_0()$.

The non-trivial solutions to the *s* wavenumbers can be obtained by making the determinant of the characteristic matrix **L** given by Eq. (1) equal to zero, i.e., $\det\left[\mathbf{L}\left(k_s^2\right)\right] = 0$. As a result, the characteristic equation which describes the propagation of the *s* waves is obtained by

$$[\Omega^2 - (k_s a)^2 - SL_{11}][1 - \Omega^2 - FL - SL_{22}] - [\mathrm{i}\nu_p(k_s a) + SL_{12}]^2 = 0 \tag{5}$$

Based on the low-frequency approximation for the Bessel function ratio and the knowledge that for the $s = 1$ wave, k_1 is much larger than the shell compressional wavenumber k_L, i.e., $k_1^2 \gg k_L^2$ [11], substitution of the fluid loading term *FL* given by Eq. (3), Eq. (5) can be rearranged to give

$$k_1^2 = k_f^2\left(1 + \frac{\beta}{1 - \Omega^2 + \alpha}\right) \tag{6}$$

where α and β are the measures of the loading effects of surrounding medium and fluid on the pipe wall, and given by $\alpha = -SL_{22} - (\nu_p - \mathrm{i}SL_{12}/k_1 a)^2/\left(1 + SL_{11}/k_1^2 a^2\right)$, $\beta = 2B_f a\left(1 - \nu_p^2\right)/E_p h$ respectively.

2.2. Loading effects of surrounding medium

Noting that the plastic pipe material is lossy by means of a complex modulus of elasticity E_p (hence a complex β), it is found from Eq. (6) that k_1 is always complex indicating the $s = 1$ wave decays as it propagates. The real and imaginary parts of the wavenumber give the propagation wavespeed and wave attenuation respectively. For plastic pipes, the fluid loading is heavy, i.e., $Re(\beta) \gg 1$. The loading effects of surrounding medium on the $s = 1$ wavenumber depend upon its elastic properties. Consider the following surrounding media:

(1) For an air medium, the loading effects of an air on the pipe wall are negligible at low frequencies. It is also referred to as an *in-vacuo* case. Assuming $\mathbf{SL} = \mathbf{0}$, the measure of the loading effects of surrounding air is reduced to a real $\alpha = -\nu_p^2$. It can be seen from Eq. (6) that at lower frequencies $\left(\Omega^2 \ll 1\right)$ the $s = 1$ wave travels significantly slower than the free-field fluid wavespeed, i.e., $k_1^2 > k_f^2$, due to the effect of heavy fluid loading, $Re(\beta) \gg 1$. Furthermore the $s = 1$ wavespeed decreases with frequency. Clearly the wave attenuation is only due to losses within the pipe wall, as can be seen from Eq. (6).

(2) For a fluid medium, the shear modulus $\mu_m \to 0$. As a result, the Lamé coefficient $\lambda_m \to B_m$ and the shear wavenumber $k_r \to \infty$ and $\mu_m k_r^2 = \omega^2\rho_m$. The loading matrix of surrounding fluid given by Eq. (4), after some manipulation, reduces to

$$SL_{11} = 0;\ SL_{12} = 0;\ SL_{21} = 0;\ SL_{22} = -\frac{\rho_m}{\rho_p}\frac{a}{h}\frac{\Omega^2}{k_{d1}^r a}\frac{H_0\left(k_{d1}^r a\right)}{\mathrm{H}_0'\left(k_{d1}^r a\right)} \tag{7a-d}$$

In this case, the measure of the loading effects of surrounding fluid reduces to a complex $\alpha = -\nu_p^2 - SL_{22}$ since SL_{22} is a function of the $s = 1$ wavenumber. Correspondingly, the wave attenuation is attributed to both material losses within the pipe wall (i.e., a complex β) and radiation losses due to the added damping of the surrounding fluid (i.e. a complex α).

(3) For a soil medium, similar to a fluid medium, the resultant wavenumber k_1 is always complex and hence a complex α. This suggests that the attenuation depends on both material losses and radiation losses. The loading matrices given by Eqs. (4) and (7) are rather cumbersome. Given a complex α for both a fluid and soil media, it is not clear from Eq. (6) how the propagation wavespeed is affected by the loading effects of surrounding medium since both real and imaginary terms contributing. Nevertheless, in simple terms, neglecting the losses, it can be seen from Eq. (6) that if the overall loading effects of surrounding fluid/soil are to add mass to the pipe wall, i.e., $Re(\alpha) < 0$, then the wavenumber will increase relative to the in-air case (corresponding to a slower wavespeed); if it is to add stiffness, i.e., $Re(\alpha) > 0$, the wavenumber will decrease compared to the in-air value (corresponding to a faster wavespeed).

3. Comparison of wavenumber predictions and measurements

This section presents some numerical results of the $s = 1$ wavenumber in comparison with the experimental data from actual MDPE water pipes. Three surrounding media are considered including an air, water and soil. Correspondingly, wavenumber measurements for the $s = 1$ wave were conducted on the in-air, in-water and buried MDPE water pipes, as shown in Figs. 3(a)–(c). The detailed information about the material properties of the actual pipe systems is given in Table 1. The tests on the in-air and in-water pipes were carried out in the laboratory while measurements on the buried water pipe were made outside at the temperature being only a few °C. Thus the elastic modulus of MDPE is given at both room-temperature and low-temperature (marked by *) in the table. The description of the test site and measurement

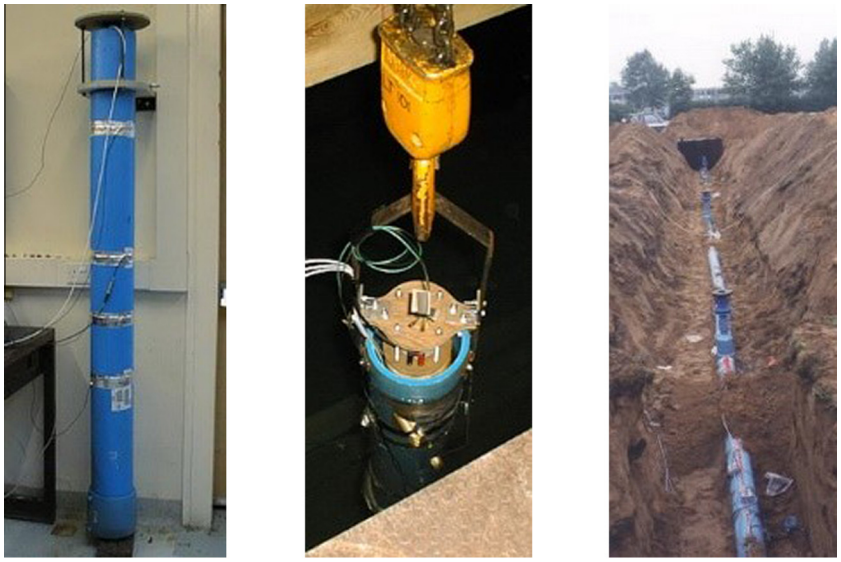

Fig. 3. Experimental set-up for wavenumber measurements on water-filled MDPE pipes: (a) in-air; (b) in-water; (c) buried in sandy soil.

Table 1
Parameters of the MDPE pipe and media.

Parameters	MDPE	Air	Water	Soil
a (m)	0.0845	–	–	–
h (m)	1.1e−2	–	–	–
Density (kg/m^3)	900	1.29	1000	1500
Young's modulus (N/m^2)	1.6 (2.0*)e9	–	–	–
Bulk's modulus (N/m^2)	–	1.42e5	2.25e9	4e7
Shear modulus (N/m^2)	–	–	–	1.5e7
Poisson's ratio	0.4	–	–	–
Material loss factor	0.06	–	–	–

* Indicates low-temperature value.

procedures are detailed in [15,18]. Here experimental results are used to validate the current theory for wavenumber predictions, and to examine the loading effects of surrounding medium, acting as a combination of mass, stiffness and radiation damping, on the pipe wall. The complex wavenumbers k_1 are calculated recursively using Eq. (6) with the loading matrix **SL** defined by Eq. (4). The real parts of the wavenumber are plotted against frequency and the imaginary parts are expressed as wave attenuation (loss) in dB/m where

$$\text{Attenuation}(\text{dB/m}) = 20\frac{\text{Im}\{k_1\}}{\ln(10)} \tag{8}$$

3.1. In-air and in-water pipes

Figs. 3(a) and (b) show the experimental set-up on a water-filled MDPE pipe, approximately 2 m in length for the in-air and in-water tests respectively. The wavenumber measurements were

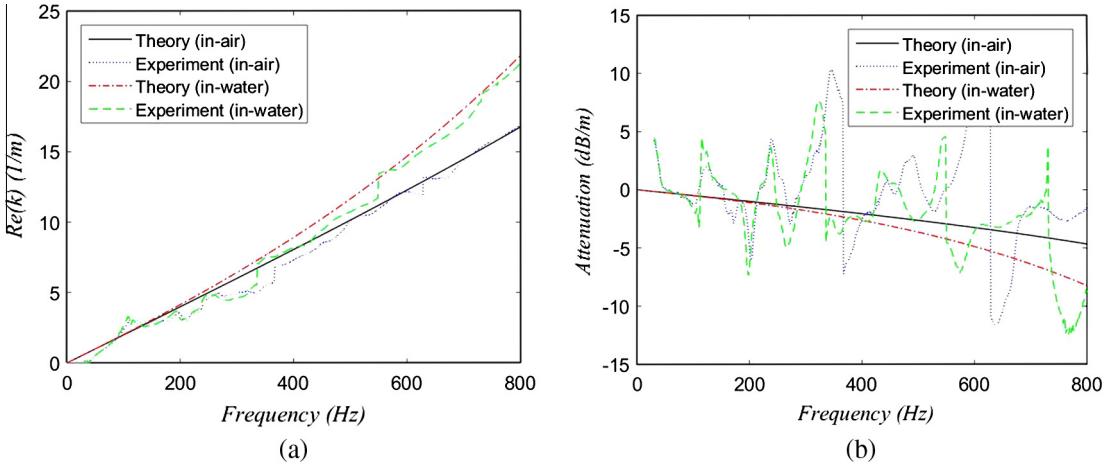

Fig. 4. Comparison of measured and predicted wavenumbers on the in-air and in-water MDPE water pipes: (a) real part; (b) attenuation (dB/m).

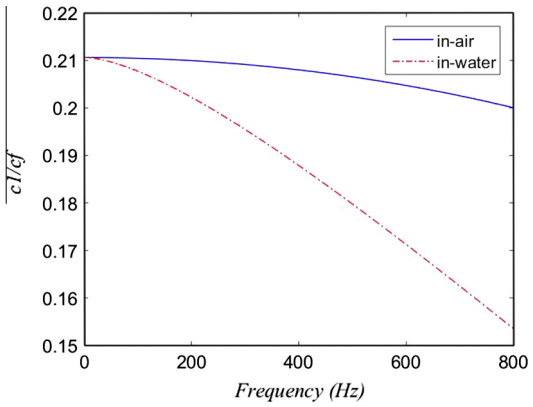

Fig. 5. Predicted wavespeeds for the $s = 1$ wave on the in-air and in-water MDPE water pipes. The wavespeeds are normalised by the free-field wavespeed c_f.

conducted using three PVDF wire ring transducers instrumented on the in-air pipe [15] and three hydrophones on the in-water pipe [18], spaced 0.5 m apart, for the pipe was not designed anechoically. Fig. 4(a) shows good agreement between the measured and predicted real parts of the wavenumber for both the in-air and in-water cases. The deviation of the measured data from the theory is caused by small errors in decomposing the outgoing and reflected waves in the pipe. As shown in the figure, there is an increase of the real part of the wavenumber for the in-water pipe relative to the in-air case. Correspondingly, the $s = 1$ wave for the in-water pipe travels slower than for the in-air pipe, as plotted in Fig. 5. For the MDPE pipes considered, the fluid loading is very heavy, $Re(\beta) = 18$, which causes a great decrease in the propagation wavespeeds relative to the free-field wavespeed c_f. It can be found in the figure that the $s = 1$ wavespeed c_1 for the in–air pipe is much less than the free-field fluid wavespeed c_f, and decreases with frequency (increasing Ω^2), as anticipated.

In order to better understand the loading effects of surrounding fluid on the dispersive behaviour of the $s = 1$ wave, the real and imaginary parts of the measure α are plotted in Figs. 6(a) and (b) respectively. As shown in the figures, for the in-air pipe, α coincides with the *in-vacuo* value $\alpha = -\nu_p^2$ (calculated as -0.16). For the in-water pipe, the level of $\mathrm{Im}(\alpha)$ is much smaller relative to $Re(\alpha)$. Thus $Re(\alpha)$ plays a dominant role in the overall loading effects of surrounding fluid on the propagation characteristics. As stated in Section 2.2, a negative $Re(\alpha)$ indicates that a fluid medium is to add mass to the pipe wall and thereby decreasing the propa-

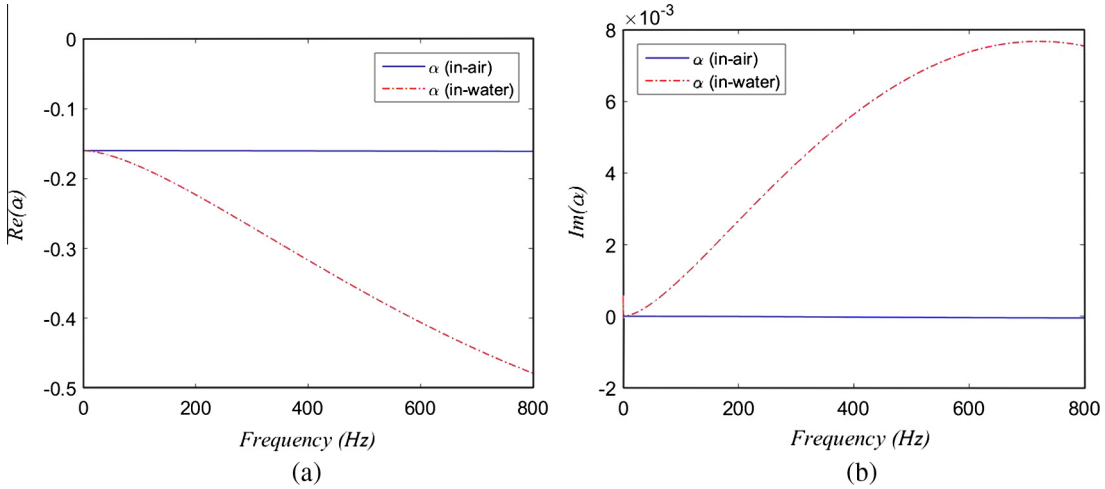

Fig. 6. Measures of the loading effects of surrounding fluid α in comparison with the in-air case: (a) real part; (b) imaginary part.

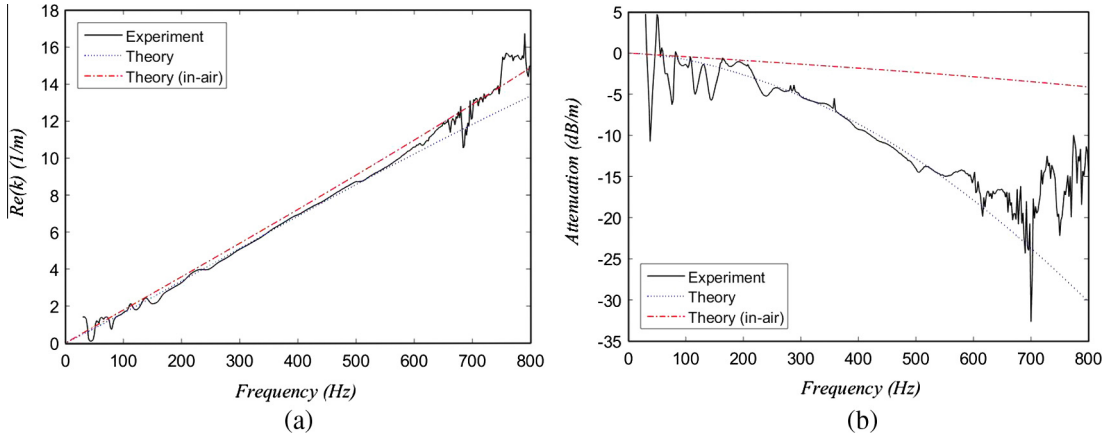

Fig. 7. Comparison of measured and predicted wavenumbers on the buried MDPE water pipe: (a) real part; (b) attenuation (dB/m).

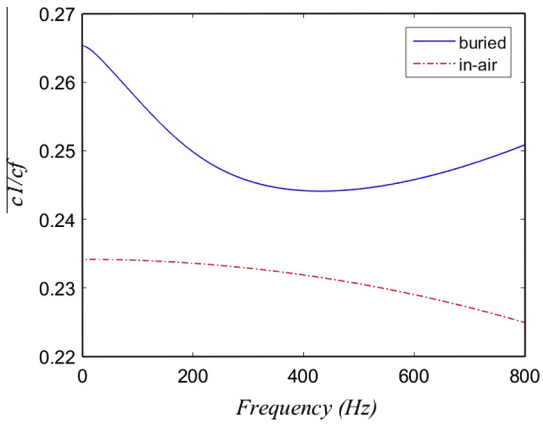

Fig. 8. Predicted wavespeeds for the $s = 1$ wave on the buried and in-air MDPE water pipes. The wavespeeds are normalised by the free-field wavespeed c_f.

gation wavespeed. It can be found in Fig. 6(a) that $Re(\alpha)$ decreases with frequency, and therefore leads to a more distinct reduction in the wavespeed at higher frequencies as plotted in Fig. 5.

Fig. 4(b) shows the attenuation on the in-air and in-water pipes. There is less agreement between the measured and predicted results compared to the real parts of the wavenumber, as a result of larger errors in the wave decomposition when calculating the imaginary parts of the wavenumber. Nevertheless, the mean values of the measured data match the theory well. As discussed in Section 2.2, for a fluid-filled pipe surrounded by an elastic medium, the attenuation can be attributed to both material losses and radiation losses. For an air medium, the attenuation is due to losses within the pipe wall and, as such, varies approximately linearly with frequency, as can be seen from the figure. When the pipe is surrounded by a fluid medium, the attenuation increases as a result of the added radiation damping. As shown in Fig. 4(b), the radiation damping effect increases with frequency. At very low frequencies (below 200 Hz) this effect is relatively small and losses within the pipe dominate whereas it increases distinguishably at higher frequencies relative to the in-air value.

3.2. Buried pipe

Fig. 3(c) shows the wavenumber measurements at a buried water pipe facility consisting of a MDPE pipe buried in loose, sandy soil. An anechoic terminator was fitted to the pipe end to reduce wave reflections in the tank. The details of the experimental setup and analysis can be found in [15] and are not reproduced in detail here. Signals from a pair of hydrophones spaced 2.02 m were used to calculate the $s = 1$ wavenumber. Figs. 7(a) and (b) show some fluctuations in both the real and imaginary parts of the measured results below 160 Hz due to some reflections from pipe connections; above 550 Hz the measured data becomes unreliable, with the "noise floor" being reached for the hydrophone pairs.

Good agreement is found in the real parts of the wavenumbers between predicted and measured for a soil medium. Upon adopting the elastic modulus of MDPE at low-temperature, the fluid loading is found to be $Re(\beta) = 14$. Fig. 7(a) shows that a slight decrease of the real part of the wavenumber (i.e. an increase of the wavespeed as plotted in Fig. 8) compared to the in-air value. This implies that the soil medium effectively acts as stiffness on the pipe wall. Additional check on the loading effects of surrounding soil on the $s = 1$ wavenumber is made by plotting the measure α. As shown in Figs. 9(a) and (b), for a buried pipe, $Re(\alpha)$ is a positive at very low frequencies where $\mathrm{Im}(\alpha)$ is considerably small. Thus the soil medium adds stiffness to the pipe wall, as expected. However, $Re(\alpha)$ turns negative with increasing frequency and gradually approaches to a significantly lower level compared to the increasing $\mathrm{Im}(\alpha)$, which in turn adds stiffness to the pipe wall along with radiation damping. By comparing Figs. 4(b) and 7(b), it can be seen that a soil medium adds larger radiation damping to the pipe wall and hence greater losses. It is observed that the attenuation in the buried water pipe increases substantially compared to the in-water case, being up to 15 dB/m for a soil and 4 dB/m for a fluid at 550 Hz. This explains that in practice, water leaks can generally be detected in plastic pipes at limited ranges.

4. Conclusions

The loading effects of surrounding medium on the propagation characteristics of the $s = 1$ wave have been investigated based on the analytical solution to the $s = 1$ wavenumber for a fluid-filled plastic pipe surrounded by an elastic medium. Examination of the form of the analytical expression has been made for an air, water and soil media. The theory presented in this paper has been applied to wavenumber measurements made previously on MDPE water pipes and good agreement has been shown for the in-air, in-water and buried cases. The model has been used to show explicitly the loading effects of surrounding medium, acting as a combination of mass, stiffness and radiation damping on the $s = 1$ wavenumber as follows

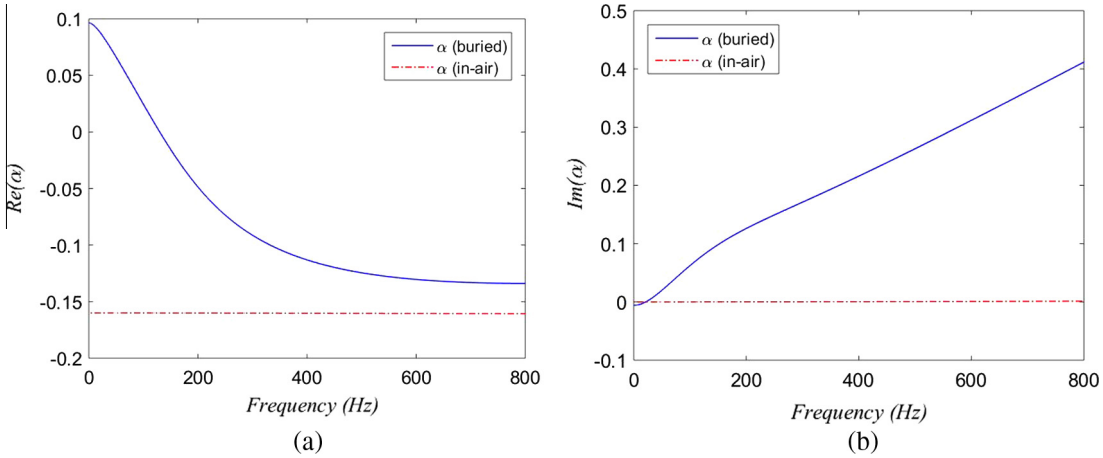

Fig. 9. Measures of the loading effects of surrounding soil α in comparison with the in-air case: (a) real part; (b) imaginary part.

- The loading effects of an air on the wavenumber are negligible at low frequencies. The wavespeed is slower than the free-field wavespeed due to the heavy fluid loading and the wave attenuation is governed by losses within the pipe wall.
- A fluid medium is to add mass to the pipe wall, and thereby decreasing the wavespeed relative to the in-air value. The attenuation is attributed to both material losses within the pipe wall and radiation losses as a result of the added radiation damping.
- A soil medium is to add stiffness and radiation damping to the pipe wall. Correspondingly, the wavespeed increases compared to the in-air case. The added damping effect is greater than that for a fluid medium, and thus leads to the largest attenuation compared to an air and water media.

The analytical method provides the framework for modelling the propagating $s = 1$ wave in a fluid-filled plastic pipe. It facilitates insight into the loading effects of surrounding medium on the propagation characteristics at low frequencies and will enable acoustic techniques to be improved for leak detection in fluid-filled pipe systems.

Acknowledgements

The authors acknowledge the support provided by the CAS Hundred Talents Programme. Many thanks are also due to the EPSRC (under EP/K0216991/1), and Professor Mike Brennan and Dr Paul Linford for providing the test data.

References

[1] Fuchs HV, Riehle R. Ten years of experience with leak detection by acoustic signal analysis. Appl Acoust 1991;33:1–19.
[2] Hunaidi O, Chu WT. Acoustical characteristics of leak signals in plastic water distribution pipes. Appl Acoust 1999;58:235–54.
[3] Hunaidi O, Wang A. A new system for locating leaks in urban water distribution pipes. J Environ Qual 2006;7(4):450–66.
[4] Khulief YA, Khalifa A, Mansour RB, Habib MA. Acoustic detection of leaks in water pipelines using measurements inside pipe. J Pipeline Syst Eng 2012;3(2):47–54.
[5] Gao Y, Brennan MJ, Joseph PF. A comparison of time delay estimators for the detection of leak noise signals in plastic water distribution pipes. J Sound Vib 2006;292:552–70.
[6] Brennan MJ, Gao Y, Joseph PF. On the relationship between time and frequency domain methods in time delay estimation for leak detection in water distribution pipes. J Sound Vib 2007;304:213–23.
[7] Lin TC, Morgan GW. Wave propagation through fluid contained in a cylindrical, elastic shell. J Sound Vib 1956;28:1165–76.
[8] Fuller CR, Fahy FJ. Characteristics of wave-propagation and energy-distributions in cylindrical elastic shells filled with fluid. J Sound Vib 1982;81:501–18.
[9] Xu MB, Zhang WH. Vibrational power flow input and transmission in a circular cylindrical shell filled with fluid. J Sound Vib 2000;234:387–403.
[10] Fuller CR. The input mobility of an infinite circular cylindrical elastic shell filled with fluid. J Sound Vib 1983;87:409–27.
[11] Pinnington RJ, Briscoe AR. Externally applied sensor for axisymmetrical waves in a fluid-filled pipe. J Sound Vib 1994;173:503–16.
[12] Pinnington RJ. The axisymmetric wave transmission properties of pressurized flexible tubes. J Sound Vib 1997;204:271–89.
[13] Pinnington RJ. Axisymmetric wave transfer functions of flexible tubes. J Sound Vib 1997;204:291–310.
[14] Muggleton JM, Brennan MJ, Pinnington RJ. Wavenumber prediction of waves in buried pipes for water leak detection. J Sound Vib 2002;249:939–54.
[15] Muggleton JM, Brennan MJ, Linford PW. Axisymmetric wave propagation in fluid-filled pipes: wavenumber measurements in in vacuo and buried pipes. J Sound Vib 2004;270:171–90.
[16] Muggleton JM, Yan J. Wavenumber prediction and measurement of axisymmetric waves in buried fluid-filled pipes: inclusion of shear coupling at a lubricated pipe/soil interface. J Sound Vib 2013;332:1216–30.
[17] Gao Y, Sui F, Muggleton JM, Yang J. Simplified dispersion relationships for fluid-dominated axisymmetric wave motion in buried fluid-filled pipes. J Sound Vib 2016;375:386–402.
[18] Muggleton JM, Brennan MJ. Leak noise propagation and attenuation in submerged plastic water pipes. J Sound Vib 2004;278:527–37.